© 2020. Published by The Company of Biologists Ltd | Journal of Cell Science (2020) 133, jcs252551. doi:10.1242/jcs.252551

SHORT REPORT

Cdc48 regulates intranuclear quality control sequestration of the Hsh155 splicing factor in budding yeast

Veena Mathew[1], Arun Kumar[1,2], Yangyang K. Jiang[1], Kyra West[1], Annie S. Tam[1,2] and Peter C. Stirling[1,2,*]

ABSTRACT

Cdc48 (known as VCP in mammals) is a highly conserved ATPase chaperone that plays an essential role in the assembly and disassembly of protein–DNA complexes and in degradation of misfolded proteins. We find that in *Saccharomyces cerevisiae* budding yeast, Cdc48 accumulates during cellular stress at intranuclear protein quality control sites (INQ). We show that Cdc48 function is required to suppress INQ formation under non-stress conditions and to promote recovery following genotoxic stress. Cdc48 physically associates with the INQ substrate and splicing factor Hsh155, and regulates its assembly with partner proteins. Accordingly, *cdc48* mutants have defects in splicing and show spontaneous distribution of Hsh155 to INQ aggregates, where it is stabilized. Overall, this study shows that Cdc48 regulates deposition of proteins at INQ and suggests a previously unknown role for Cdc48 in the regulation or stabilization of splicing subcomplexes.

This article has an associated First Person interview with the first author of the paper.

KEY WORDS: Protein quality control, Cdc48, INQ, Hsh155, Splicing, Yeast

INTRODUCTION

Protein quality control (PQC) refers to the process of triage for non-native, unassembled or mislocalized proteins through a combination of sequestration, degradation and refolding (Hartl et al., 2011). PQC is a part of normal cellular homeostasis and is particularly important during stress, when non-native proteins assemble in visible aggregate structures at different subcellular locations. Various proteotoxic stresses elicit such a coordinated PQC response, with the best characterized of these being heat stress (Wallace et al., 2015) and expression of amyloid-forming proteins (Kaganovich et al., 2008). PQC responses depend on networks of molecular chaperones, on the action of stress-activated protein aggregase and disaggregase activities (Hartl et al., 2011) and on protein degradation by the ubiquitin–proteasome system and autophagy (Kaganovich et al., 2008; Kumar et al., 2016).

During stress in yeast, specific types of aggregate structures with different components and behaviors form (Saarikangas and Barral, 2016). In the cytoplasm, aggregates at the vacuolar membrane, called the insoluble protein deposit (IPOD), are repositories for irreversibly aggregated proteins destined for degradation, such as amyloids (Kaganovich et al., 2008). Smaller dynamic cytoplasmic aggregates called Q-bodies (quality control bodies) have also been described for protein aggregate reporters such as the temperature-sensitive mutant Ubc9-ts and VHL (Escusa-Toret et al., 2013; Ruan et al., 2017; Zhou et al., 2014). Finally, at the nuclear envelope, the juxtanuclear quality control site (JUNQ) forms peripheral to but outside the nucleus, whereas the intranuclear quality control site (INQ) forms peripheral to and inside the nucleus (Kaganovich et al., 2008; Miller et al., 2015). Most yeast studies of PQC focus on aggregation of the replication fork checkpoint proteins (i.e. Mrc1; Gallina et al., 2015), the activation of DNA repair proteins (i.e. Mus81; Saugar et al., 2017) or rewiring of the spliced transcriptome (i.e. Hsh155; Mathew et al., 2017).

INQ formation is driven by the small heat shock protein Hsp42 and the aggregase protein Btn2 (Ho et al., 2019), whereas INQ dissolution is regulated by Hsp104 and the Hsp70 system (Miller et al., 2015; Saugar et al., 2017). Here, we show that Cdc48 is also a stress-inducible component on INQ structures and that it plays an enzymatic role in INQ turnover. Cdc48 plays numerous normal and stress-responsive roles in cells, including in nuclear PQC (Gallagher et al., 2014; Maric et al., 2017; Pantazopoulou et al., 2016; Verma et al., 2011). Here, we show that Cdc48 is concentrated at INQ following DNA damage, and that its activity is important to suppress the spontaneous aggregation of splicing factor Hsh155 in INQ. Cdc48 physically interacts with Hsh155, even under non-stress conditions, and promotes its assembly with partners in the SF3B complex of the spliceosome. Taken together, these results demonstrate a previously unrecognized role for Cdc48 in protein triage to INQ and suggest unappreciated roles for Cdc48 in splicing.

RESULTS AND DISCUSSION

Cdc48–GFP localizes to intranuclear quality control sites

We previously screened hundreds of genome stability regulatory proteins for relocalization in response to DNA damage, and identified uncharacterized stress-induced relocalization of Cdc48–GFP (Mathew et al., 2017). Cdc48 is widely distributed in unstressed cells, but is enriched at a nuclear periphery/ER localization due to its role in ER-associated degradation (ERAD) (Fig. 1A). Following methyl methanesulfonate (MMS) treatment, Cdc48 relocalized to nuclear and non-nuclear foci (Fig. 1A; Fig. S1A). To test whether these foci were INQ, we expressed Cdc48–GFP together with Hos2–mCherry, a known marker of INQ (Gallina et al., 2015; Tkach et al., 2012). Cdc48–GFP foci colocalized with Hos2–mCherry foci, suggesting that Cdc48 was accumulating at INQ following MMS treatment (Fig. 1B,C). Cdc48 also colocalized with Hos2 at peripheral aggregates, which may be cytoplasmic PQC (CytoQ) sites (Fig. 1B,C). We next ablated INQ formation by deleting the chaperones *HSP42* and

[1]Terry Fox Laboratory, British Columbia Cancer Agency, Vancouver V5Z 1L3, Canada. [2]Department of Medical Genetics, University of British Columbia, Vancouver V6H 3N1, Canada.

*Author for correspondence (pstirling@bccrc.ca)

P.C.S., 0000-0003-2651-4539

Handling Editor: Maria Carmo-Fonseca
Received 31 July 2020; Accepted 30 October 2020

Journal of Cell Science (2020) 133, jcs252551. doi:10.1242/jcs.252551

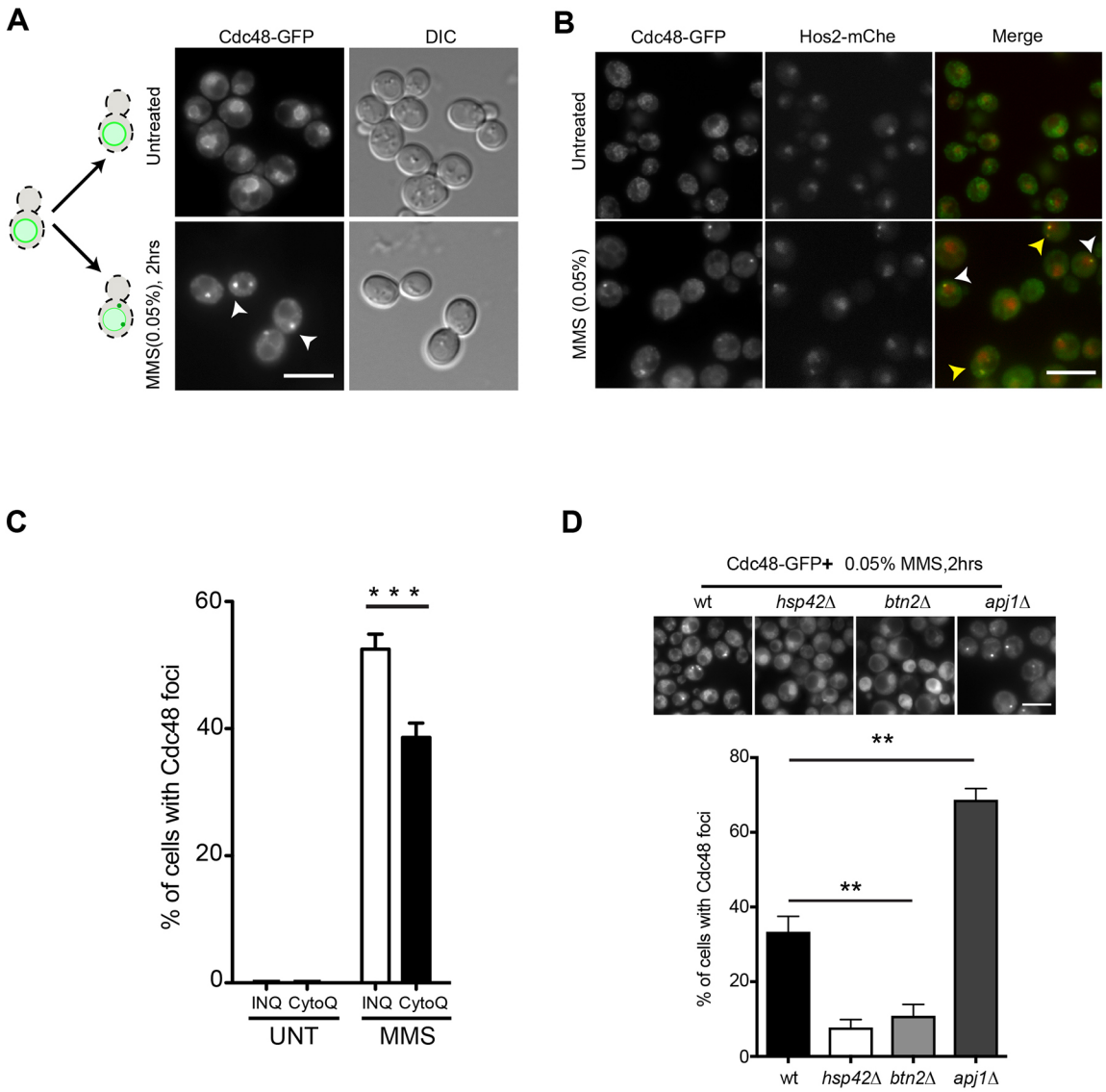

Fig. 1. Cdc48 localizes to PQC structures in a chaperone-dependent manner. (A) Cdc48–GFP fusions relocalize into foci upon MMS treatment (white arrowheads). A schematic on left summarizes the movements in both conditions. (B) Cdc48–GFP foci overlap with Hos2–mCherry (mChe) foci after MMS treatment. White arrowheads indicate INQ foci, yellow arrowheads indicate CytoQ foci. (C) Quantification of MMS-induced Cdc48 in perinuclear (INQ) and peripheral (CytoQ) foci. Data are presented as mean±s.e.m., *n*=3 with >100 cells each. UNT, untreated. ***P<0.001 (Fisher test). (D) Reduction of Cdc48–GFP foci in MMS-treated cells lacking *HSP42* (*hsp42*Δ) or *BTN2* (*btn2*Δ), and increase of Cdc48–GFP foci in *apj1*Δ cells, compared with those in MMS-treated wild-type cells (wt). Representative images (top) and quantification of percentage of cells with foci (bottom) are shown. Data are presented as mean±s.e.m., *n*=3 with >50 cells each. **P<0.01 (Fisher test). Asterisks show P-value thresholds in comparison to WT under the same condition. Scale bars: 5 µm.

BTN2, which are essential for INQ protein localization (Gallina et al., 2015; Mathew et al., 2017; Miller et al., 2015). Cdc48–GFP foci were strongly diminished in MMS-treated *hsp42*Δ or *btn2*Δ cells, showing that INQ formation was essential for Cdc48 foci (Fig. 1D; Fig. S1B). In contrast, deletion of the Hsp40 homolog Apj1, which has previously been implicated in disaggregation and turnover of INQ-resident proteins, dramatically increased the frequency of Cdc48–GFP foci (Fig. 1D; Fig. S1B) (den Brave et al., 2020). Hos2–mCherry was used as a control, and it showed the expected decrease of INQ formation in cells lacking *HSP42* or *BTN2* and increased INQ frequency in cells lacking *APJ1* (Fig. S1B). Taken together, the results of these experiments suggest that Cdc48 foci mark INQ structures induced by MMS treatment and are influenced by INQ regulatory chaperones.

Cdc48 ATPase regulates the aggregation and INQ localization of Hsh155

Because Cdc48 functions in protein biogenesis and turnover, we suspected that it might have a functional role at INQ. We assembled a set of *CDC48* temperature-sensitive alleles, which grew robustly at the permissive temperature of 25°C but exhibited a range of fitness defects (Fig. S1C) (Li et al., 2011). Examining the localization of an INQ substrate in the most severe allele, *cdc48-4601* (hereafter called *cdc48-4*) (Fig. S1E), revealed spontaneous Hsh155–GFP and Hos2–GFP foci at nuclear and cytoplasmic aggregate sites (Fig. 2A; Fig. S1D). MMS treatment further increased the proportion of cells with visible aggregates beyond that seen for MMS-treated wild-type (WT) cells (Fig. 2B). We confirmed that other *CDC48* temperature-sensitive alleles also increased spontaneous INQ formation to varying degrees (Fig. 2C).

Journal of Cell Science (2020) 133, jcs252551. doi:10.1242/jcs.252551

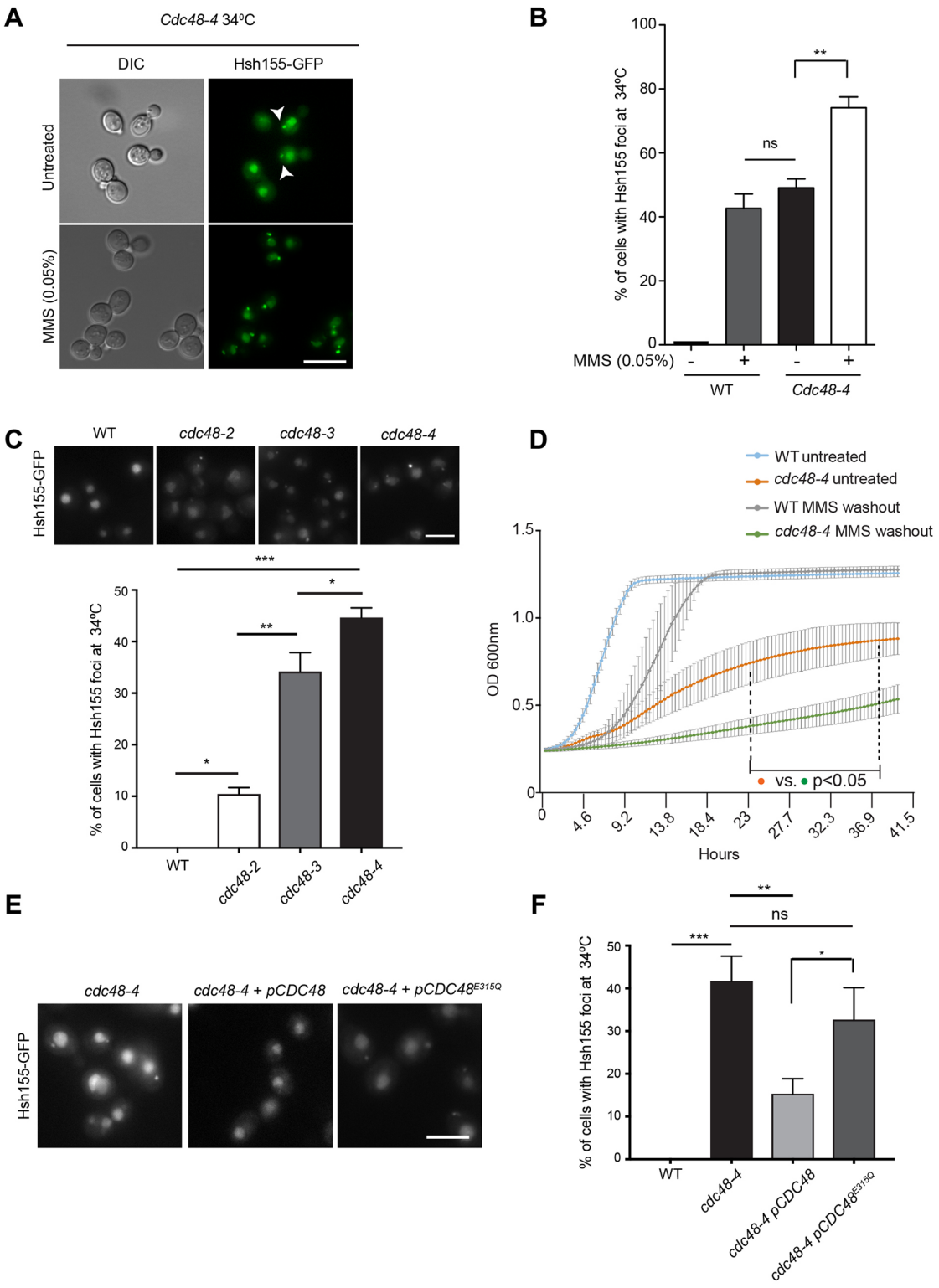

Fig. 2. Cdc48 ATPase regulates the aggregation and INQ localization of Hsh155. (A) Visualization of Hsh155–GFP foci in cells with temperature-sensitive alleles of *CDC48* (*cdc48-4*) with or without MMS stress at 34°C. White arrowheads show foci in untreated cells. (B) Quantification of foci accumulation in untreated and MMS-treated *cdc48-4* cells compared with that in WT cells with or without MMS. (C) Spontaneous Hsh155–GFP foci in three different *CDC48* mutant alleles at 34°C. Representative images (top) and quantification (bottom) are shown. (D) Growth curve analysis of *cdc48-4* after 2 h of MMS treatment and washout compared with untreated *cdc48-4* cells and WT with or without MMS treatment and washout at 34°C. Data are presented as mean±s.e.m., *n*=3 with triplicates in each. The dotted lines represent the interval wherein all *cdc48-4* data points significantly differ from WT after MMS washout (*P*-value ranges from *P*<0.05–*P*<0.0001) and where data points for untreated and treated *cdc48-4* cells significantly differ from each other (P<0.05). *T*wo-way ANOVA with Tukey's post hoc test. (E,F) Rescue of Hsh155–GFP foci formation by WT *CDC48* but not by the *CDC48*^{E315Q} ATPase-deficient allele. E is a representative image of data quantified in F. For B,C and F quantifications: data are presented as mean±s.e.m., *n*=3 with >50 cells each. ***P<0.001; **P<0.01; *P<0.05; ns, not significant (Fisher test). Scale bars: 5 µm.

Consistent with a functionally important role, *cdc48-4* alleles were significantly impaired in recovery from a 2 h treatment of MMS (Fig. 2D). Although there are many possible mechanisms for the MMS sensitivity of a *CDC48* temperature-sensitive allele, our data show that Cdc48 function is important for regulating the INQ localization of Hsh155 in normal and DNA-damaging conditions. Finally, because Cdc48 uses its ATPase activity to disassemble or unfold proteins, we tested the ability of enzymatically active or dead alleles to rescue the *cdc48-4* phenotype. Whereas WT *CDC48* plasmids suppressed Hsh155 foci, an ATPase-deficient $CDC48^{E315Q}$ allele could not (Fig. 2E,F) (Gallagher et al., 2014). Thus, Cdc48 ATPase activity is essential to suppress aggregation of Hsh155–GFP into INQ structures.

SUMOylation regulates INQ formation in *cdc48* mutants

Previous studies have linked Cdc48 and its co-factors to proteostasis of nuclear proteins via the San1 E3 ubiquitin ligase and the inner nuclear membrane proteins Asi1–Asi3; however, we saw no significant effect of *SAN1* deletion on INQ (Fig. S1F) (Gallagher et al., 2014; Pantazopoulou et al., 2016). In addition, Cdc48 is involved in regulation of protein–DNA complexes, including the removal of RNA polymerase from damaged DNA (Verma et al., 2011), the removal of replisomes during DNA replication termination (Maric et al., 2017), at protein–DNA crosslinks (Amunugama et al., 2018) and during the release of condensin complexes (Thattikota et al., 2018). Thus, Cdc48 is well-positioned to regulate protein sequestration pathways such as INQ formation following DNA damage detection. Other groups have noted the importance of SUMO to INQ formation (Gallina et al., 2015), and we also found that reducing SUMOylation with *ubc9-ts* (SUMO E2) or *SIZ1* (SUMO E3) deletion reduced INQ localization of Hsh155–GFP in MMS-treated WT or *cdc48-4* cells (Fig. 3A,B). Indeed, mutation of the SUMO-interacting motif of Cdc48 ($CDC48^{SIM}$) impairs its ability to rescue *cdc48-4* cells, relative to rescue by WT *CDC48* (Fig. 3C) (Bergink et al., 2013). Because we used Hsh155–GFP as a marker for INQ, we elected to directly test whether Hsh155 is SUMOylated using a Smt3–His×7 purification scheme. Whereas SUMOylation of the Rfa1–GFP control was easily detectable upon MMS treatment, no detectable pulldown of Hsh155–GFP with an Smt3–His×7 tag was observed with or without MMS (Fig. 3D). Thus, the identity of any SUMO targets important for regulating INQ will require additional study beyond the scope of this work. However, our findings again highlight the importance SUMO in regulating INQ.

Cdc48 regulates the stability of Hsh155 and assembly with its partners

If Cdc48 is important for the prevention or dissolution of INQ structures, then it could regulate the stability of INQ substrate proteins under stress. Consistent with this idea, Hsh155–GFP protein was more abundant in the *cdc48-4* mutant, and more stable in cycloheximide chase experiments, than it was in WT (Fig. 4A). Because cycloheximide treatment can itself affect protein sequestration (Zhou et al., 2014), we also monitored the impact of Cdc48 on Hsh155 lifetime with an orthogonal approach using *in vivo* tandem fluorescent timer (tFT) fusions (Khmelinskii et al., 2012). The ratio of GFP to mCherry fluorescence in Hsh155–tFT fusions was significantly red-shifted in *cdc48-4* cells, indicating a longer relative protein lifetime (Fig. 4B; Fig. S1G,H). These data are consistent with INQ serving a protective role for substrate proteins, because Hsh155 both becomes more abundant and aggregates in *cdc48-4* cells. Cdc48 could affect the stability of Hsh155 through direct protein–protein interactions. Indeed, we observed co-precipitation of Hsh155–GFP with Cdc48–TAP and via reciprocal pulldown (i.e. Cdc48–GFP with Hsh155–TAP) under both untreated and MMS-treated conditions (Fig. 4C,D).

Hsh155 is a splicing factor that exists in a complex called SF3B with Hsh49 and Cus1. We previously found that Hsh155 disassembles from the SF3B complex upon MMS treatment (Mathew et al., 2017). To assess the potential impact of Cdc48 on SF3B complex stability, we monitored pulldown of Hsh155–GFP in WT and *cdc48-4* cells with or without MMS treatment using co-immunoprecipation. Loss of Cdc48 function greatly diminished the presence of the Hsh155–Cus1 complex, even in untreated cells (Fig. 4E). This suggests that Cdc48 may play a role in the integrity of the SF3B complex even in the absence of DNA-damage signals. Whereas *cdc48-4* grew too poorly to easily monitor splicing activity, the *cdc48-3* allele that showed an intermediate induction of Hsh155 foci (Fig. 2C) did show reduced splicing flux in a *LacZ*-based splicing efficiency assay (Fig. 4F) (Galy et al., 2004; Tam et al., 2019).

Context and perspective

Spatial control of PQC is a fundamental feature of stress responses in eukaryotic cells (Sontag et al., 2014). Here, we show that Cdc48, a key regulator of numerous cellular PQC activities, is also associated with INQ, where it interacts with, reduces the accumulation of, or speeds the turnover of the INQ substrate Hsh155 (Fig. 4G). This defines a novel and complementary function for Cdc48 in nuclear protein quality control. Loss of SUMO-conjugating enzyme function or E3 SUMO ligase function reduced INQ formation, consistent with a role for this modification in organized INQ structures. Considerably more work is needed to understand the regulation of INQ substrate protein localization and turnover. Our data specifically implicate Cdc48 in regulating the sequestration, complex formation and stability of the spliceosomal protein Hsh155 within the SF3B complex. We previously found that Hsh155 sequestration may regulate ribosomal protein gene expression through reduced splicing efficiency of ribosomal protein gene transcripts (Mathew et al., 2017). In this regard, it is notable that Cdc48 is also a critical regulator of ribosomal quality control mechanisms and can sense ribosomal stress (Brandman et al., 2012; Defenouillère et al., 2013). It is possible that these responses are coordinated during the DNA-damage response. Regardless, our data define a new function for Cdc48 in regulating the deposition of proteins at the INQ and potentially in the regulation of splicing complexes.

There is currently little evidence linking Cdc48 to splicing. Interestingly, a study of motor neuron transcriptome dynamics in induced pluripotent stem cell differentiation models of amyotrophic lateral sclerosis (ALS), where *VCP* (the human ortholog of *CDC48*) was mutated, showed that abnormal intron retention events are increased in *VCP*-mutated cells (Luisier et al., 2018). Thus, a role for Cdc48/VCP in splicing across species is possible, and we hope that additional research will elucidate how Cdc48 may affect splicing. In this regard, it is notable that the existence of an orthologous human intranuclear quality control response could involve disease genes, including the ALS gene *VCP* and the Hsh155 ortholog SF3B1, which is frequently mutated in various types of cancer (Yoshida and Ogawa, 2014). Given the proximity of the INQ to the nucleolus, we speculate that human studies highlighting the nucleolus as a phase-separated quality control compartment may reflect a conserved phenomenon homologous to the INQ in yeast (Frottin et al., 2019; Tkach et al., 2012). If so, then studies in model

Journal of Cell Science (2020) 133, jcs252551. doi:10.1242/jcs.252551

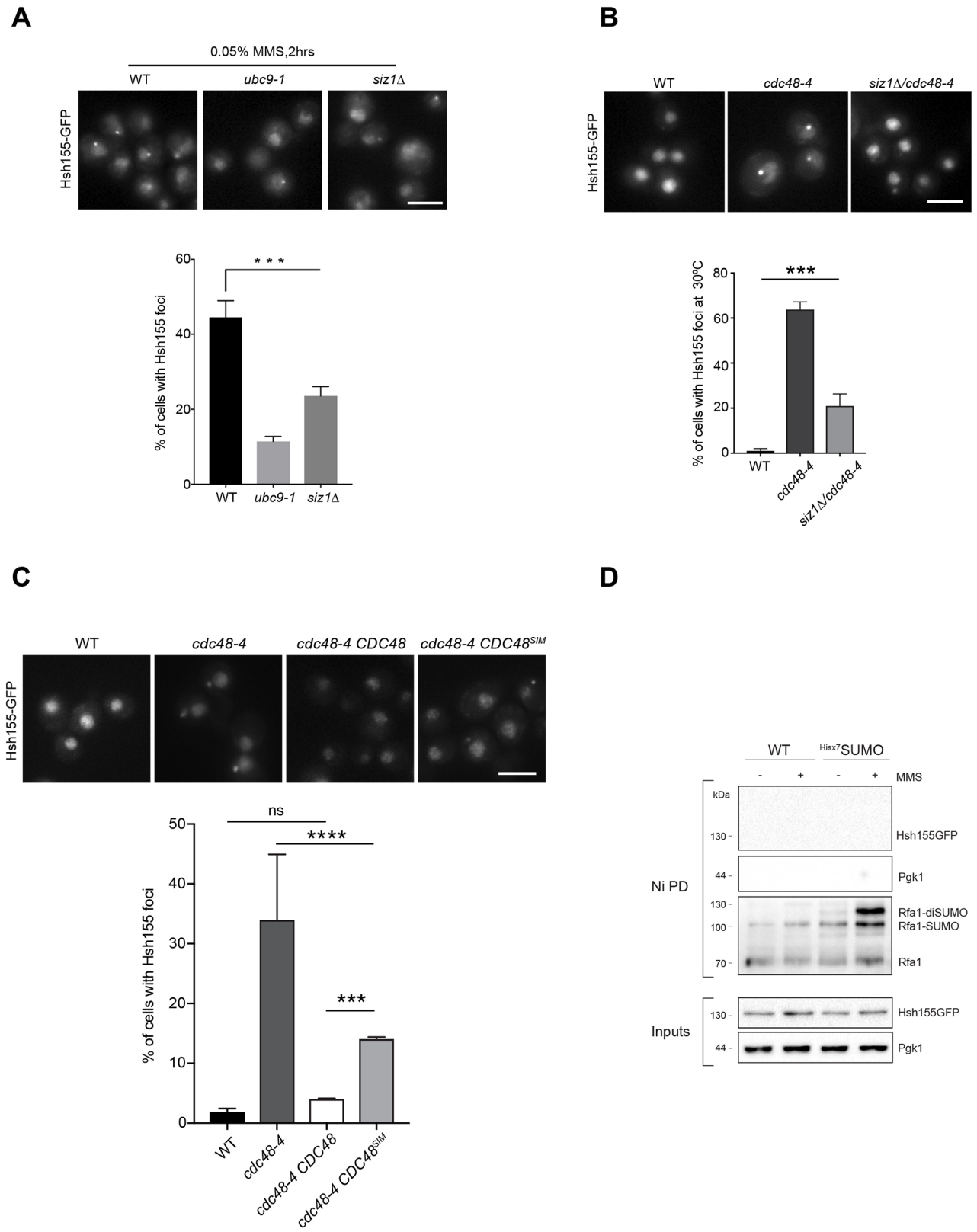

Fig. 3. Testing potential roles of SUMO in Cdc48-induced Hsh155–GFP foci formation. (A) Hsh155–GFP foci induction by MMS in SUMO regulator mutant strains *ubc9-ts* and *siz1*Δ. (B) Induction of spontaneous Hsh155–GFP foci in *cdc48-4* is reduced by deletion of SUMO E3 ligase *SIZ1*. (C) Spontaneous Hsh155–GFP foci in *cdc48-4* complemented by plasmids bearing WT *CDC48* or the *CDC48*^{SIM} mutant. For A–C, representative images (top) and quantification (bottom) are shown. Data are presented as mean±s.e.m., n=3 with >50 cells each. ****P<0.0001; ***P<0.001; ns, not significant (Fisher test). (D) SMT3–His×7 ($^{His\times7}$SUMO) pulldown assays in untreated or MMS-treated WT and SMT3–His×7-expressing cells. DNA-damage induced SUMOylation of RFA1 in MMS (Psakhye and Jentsch, 2012) is shown as a positive control after Ni-NTA bead pulldown (Ni PD). No bands are detectable when blotting for Hsh155–GFP. Pgk1 is shown as a loading control for input. Input, 4%. Scale bars: 5 µm.

Journal of Cell Science (2020) 133, jcs252551. doi:10.1242/jcs.252551

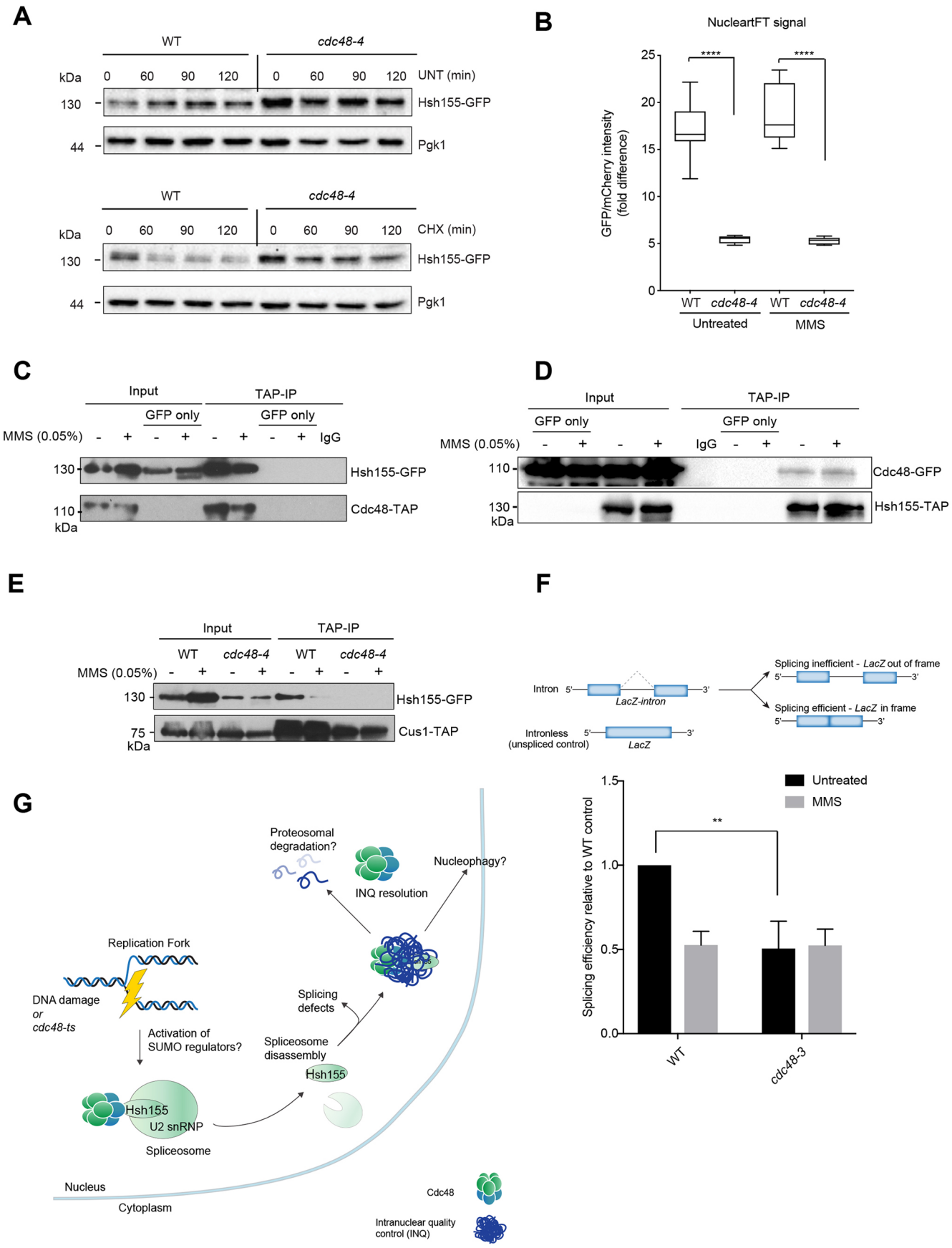

Fig. 4. See next page for legend.

Fig. 4. Direct effects of Cdc48 on Hsh155 stability and function. (A) Hsh155 protein levels with or without cycloheximide treatment for the indicated times, assayed by anti-GFP western blotting in WT and *cdc48-4* cells, relative to Pgk1 levels. CHX, cycloheximide; UNT, untreated. A representative blot from three independent experiments is shown. (B) Tandem fluorescent timer (tFT) analysis of Hsh155–mCherry–GFP dual fusion lifetime in the indicated strains with or without MMS treatment. Ratios of GFP (fast maturing) to mCherry (slow maturing) fluorescence in the nucleus are shown. Quantification of the fluorescent timer indicates the presence of older proteins in the nucleus of *cdc48-4* cells compared to those in WT in both conditions. Representative images are shown in Fig. S1G. Box plots show the median and interquartile range, with whiskers indicating the minimum and maximum values. Three replicates, $n \geq 30$ per replicate. ****$P<0.0001$ (Mann–Whitney test). (C,D) Physical interaction of Hsh155 and Cdc48 with or without MMS treatment, as assayed by co-immunoprecipitation (IP) using Cdc48–TAP (C) or Hsh155–TAP (D) followed by western blotting. Control (GFP only) lanes are IgG bead IPs from otherwise isogenic cells expressing Hsh155–GFP or Cdc48–GFP without a TAP fusion to account for any non-specific binding. The IgG bead lane is a no lysate control for the beads. Input, 5%. (E) Co-precipitation of Hsh155 with its partner Cus1 in the SF3B complex in *cdc48-4* cells is disrupted in both untreated and MMS conditions, similar to MMS-induced WT cells. Input, 5%. (F) *LacZ* splicing reporter assay results in WT or *cdc48-3* cells treated with MMS. Top: a schematic of the assay (top) shows the intronic versus intronless *LacZ* constructs that enable quantification of splicing efficiency. Bottom: quantification of relative *LacZ* splicing in untreated and MMS-treated conditions, normalized to the WT 'no intron' control, in both WT and *cdc48-3* cells. Data are presented as mean±s.e.m., $n=5$ with triplicate individual transformants in each. **$P<0.01$ (Student's *t*-test). (G) Model of Cdc48 as a chaperone for Hsh155 involved in its quality control and sequestration at INQ sites. Cdc48 binds Hsh155 under normal conditions, but its disruption or DNA damage leads to SF3B disassembly. Cdc48 may also play a role in INQ resolution or turnover, explaining why its loss increases INQ formation.

organisms should provide insight to nuclear protein quality control pathways that could modulate human disease.

MATERIALS AND METHODS

Yeast strains, MMS treatments and growth analyses

Yeast (*Saccharomyces cerevisiae*) strains used in this study, including database IDs and genotypes, primers and plasmids, are listed in Table S1. All strains were in the s288c background and were grown under nutrient rich YPD medium (Sherman, 2002) or synthetic medium lacking amino acids (SC; Sherman, 2002) unless otherwise indicated. Schematics of the *CDC48* mutant alleles are shown in Fig. S1E. Sequence information came from in-house sequencing or from publications (Simões et al., 2018; Verma et al., 2011). Serial dilution assays and growth curve analyses were performed as described previously (Mathew et al., 2017; Stirling et al., 2011). Briefly, cells with identical optical density (OD) were serially diluted tenfold and spotted on YPD plates using a 48-pin replica pinning manifold then incubated at the indicated temperatures for 72 h. Growth curves were analyzed in a Tecan M200 plate reader monitoring OD600 nm every 30 min for 48 h at 30°C. For all MMS treatment conditions cells were exposed to 0.05% MMS (~99%; Sigma) in synthetic complete medium for 2 h unless otherwise noted. For growth curves, MMS was then washed out and replaced with fresh medium.

Live-cell imaging, image acquisition, analysis and statistical methods

Imaging and subsequent analysis were performed as described previously (Mathew et al., 2017). Log-phase yeast were mounted on slides pre-treated with concanavalin A, in SC growth medium. Immobilized cells were imaged using an Objective HCX PL APO 1.40 NA oil immersion 100× objective on an inverted Leica DMi8 microscope with a motorized DIC (differential interference contrast) turret (for DIC imaging) and a filter cube set for FITC/TRITC (for GFP and mCherry fluorescence imaging). The images were captured at room temperature using a scientific complementary metal oxide semiconductor (sCMOS) camera (ORCA Flash 4.0 V2; Hamamatsu), collected using MetaMorph Premier acquisition software and post processed [including gamma adjustments, counting of cells with/without foci and foci intensity measurements for tandem fluorescent timer (tFT) experiments] using ImageJ (National Institutes of Health). For all microscopy experiments, the significance of the differences was determined using Prism version 5 or higher (Graphpad). For foci intensity measurements in tFT experiments, samples were compared with *t*-tests or ANOVA; Prism performs *F*-tests for variance as part of this analysis. For comparisons of proportions, Fisher tests were used, and *P*-values were Holm–Bonferroni corrected in the event of multiple comparisons. Sample sizes and specific statistical details for each image analysis are listed in the figure legends.

Co-immunoprecipitation and western blotting

Co-immunoprecipitation was performed using yeast strains containing TAP tagged Cus1, Cdc48 and/or GFP tagged Hsh155, treated with or without MMS. TAP-tagged protein was captured using IgG sepharose fast flow beads (Sigma) and proceeded as described previously (Leung et al., 2016). Immunoblotting was carried out with mouse anti-GFP (1:500; ThermoFisher; Cat#. MA5-15256) and rabbit anti-TAP (1:1000; ThermoFisher; Cat#. CAB1001) antibodies. For western blotting, whole-cell extracts were prepared using tricholoroacetic acid (TCA) extraction and blotted with mouse anti-GFP, rabbit anti-RFA (1:1000; Agrisera; Cat#. AS07 214) or mouse anti-PGK1 (1:500; Santa Cruz; Cat#. Sc130335) antibodies, as described previously (Gallina et al., 2015).

Protein stability timecourse

Overnight cultures of the indicated strains were diluted to below an OD600 nm of 0.2 and allowed to progress into logarithmic phase before collection. The cells were treated with or without cycloheximide (CHX) at a concentration of 200 µg/ml for the indicated times (0–120 min). The final samples of 2×10^7 cells were collected by centrifugation, and whole-cell extracts were prepared by TCA extraction and used for immunoblotting.

Splicing efficiency assay

The splicing assay protocol was adapted and performed as described previously (Galy et al., 2004). All measurements were taken with three individual transformants per replicate for a total of five replicates. Cells were struck as a patch on SC –leucine plates, then replica plated to glycerol–lactate-containing SC medium (1.6% v/v glycerol and 1.5% w/v lactate) without leucine (GGL −leu). Cells from each patch were inoculated in liquid GGL −leu medium for 2 h at 34°C and induced with galactose (2% final concentration) for 1.5 h before treatment with MMS (0.05% final concentration) for 30 min. Cells were lysed and assayed for β-galactosidase using a Gal-Screen β-galactosidase reporter gene assay system for yeast or mammalian cells (Applied Biosystems), as per the manufacturer's instructions, and read with SpectraMax i3 (Molecular Devices). Relative light units were normalized to cell concentration as estimated by measuring OD600.

Ni-NTA pulldown of SUMOylated proteins

SUMO-conjugated proteins were detected by performing protein pulldowns under denaturing conditions, as described previously (Ulrich and Davies, 2009). In brief, strains of interest were transformed with a plasmid containing His-tagged SUMO (Smt3–His×7; Addgene) under the control of a copper-inducible promoter. Logarithmically growing cells were harvested at an OD600 nm of 0.6–0.8, and a total of 10^9 cells were collected by centrifugation (4000 rpm, 3724 ***g***; 5 min at 4°C). Pelleted cells were washed and resuspended in 5 ml of pre-chilled water. Cells were then lysed with 800 µl of 1.85 M NaOH containing 7.5% (v/v) 2-mercaptoethanol, followed by 20 min incubation on ice. Protein precipitation was carried out by adding 800 µl 55% TCA on ice for 20 min. Precipitates were collected by centrifugation (8000 ***g***, 20 min, 4°C) and were resuspended in 1 ml Buffer A (6 M guanidine hydrochloride, 100 mM sodium phosphate and 10 mM Tris-HCl, pH 8.0) and incubated on a rotating block at room temperature for 1 h to solubilize the precipitate completely. The resulting solution was then centrifuged (16,000 ***g***, 10 min, 4°C), and supernatant was transferred to tubes containing 30 µl precleared Ni-NTA agarose beads (Qiagen) in the presence of 0.05% Tween-20 and 15 mM imidazole. These were incubated overnight on a rotating block at room temperature. Following binding, the

beads were washed twice with Buffer A containing 0.05% Tween-20 and four times with Buffer C (8 M urea, 100 mM sodium phosphate and 10 mM Tris-HCl, pH 6.3) containing 0.05% Tween-20. Beads were centrifuged (200 ***g***, 15 s) and supernatant was completely removed. His–SUMO conjugates on the beads were eluted by adding 30 µl HU sample buffer (8 M urea, 5% SDS, 200 mM Tris-HCl, pH 6.8, 0.1 mM EDTA, 0.5% Bromophenol Blue and 15 mg/ml dithiothreitol) and heating at 70°C for 10 min. Resultant protein extracts were subjected to standard western blotting and probed for SUMO and other proteins of interest using antibodies as described above.

Competing interests

The authors declare no competing or financial interests.

Author contributions

Conceptualization: V.M., P.C.S.; Methodology: V.M., A.K.; Investigation: V.M., A.K., Y.K.J., K.W., A.S.T.; Writing - original draft: V.M., P.C.S.; Writing - review & editing: V.M., P.C.S.; Visualization: A.K., A.S.T., P.C.S.; Supervision: P.C.S.; Project administration: P.C.S.; Funding acquisition: P.C.S.

Funding

P.C.S. is funded by a Natural Sciences and Engineering Research Council of Canada Discovery grant and Discovery Accelerator Supplement (RPGIN 2020-04360), and a Canadian Institutes of Health Research Project grant (MOP136982). P.C.S. is a Canadian Institutes of Health Research New Investigator and Michael Smith Foundation for Health Research Scholar.

Supplementary information

Supplementary information available online at
https://jcs.biologists.org/lookup/doi/10.1242/jcs.252551.supplemental

Peer review history

The peer review history is available online at
https://jcs.biologists.org/lookup/doi/10.1242/jcs.252551.reviewer-comments.pdf

References

Amunugama, R., Willcox, S., Wu, R. A., Abdullah, U. B., El-Sagheer, A. H., Brown, T., McHugh, P. J., Griffith, J. D. and Walter, J. C. (2018). Replication fork reversal during DNA interstrand crosslink repair requires CMG unloading. *Cell Rep.* **23**, 3419-3428. doi:10.1016/j.celrep.2018.05.061

Bergink, S., Ammon, T., Kern, M., Schermelleh, L., Leonhardt, H. and Jentsch, S. (2013). Role of Cdc48/p97 as a SUMO-targeted segregase curbing Rad51-Rad52 interaction. *Nat. Cell Biol.* **15**, 526-532. doi:10.1038/ncb2729

Brandman, O., Stewart-Ornstein, J., Wong, D., Larson, A., Williams, C. C., Li, G.-W., Zhou, S., King, D., Shen, P. S., Weibezahn, J. et al. (2012). A ribosome-bound quality control complex triggers degradation of nascent peptides and signals translation stress. *Cell* **151**, 1042-1054. doi:10.1016/j.cell.2012.10.044

Defenouillère, Q., Yao, Y., Mouaikel, J., Namane, A., Galopier, A., Decourty, L., Doyen, A., Malabat, C., Saveanu, C., Jacquier, A. et al. (2013). Cdc48-associated complex bound to 60S particles is required for the clearance of aberrant translation products. *Proc. Natl. Acad. Sci. USA* **110**, 5046-5051. doi:10.1073/pnas.1221724110

den Brave, F., Cairo, L. V., Jagadeesan, C., Ruger-Herreros, C., Mogk, A., Bukau, B. and Jentsch, S. (2020). Chaperone-mediated protein disaggregation triggers proteolytic clearance of intra-nuclear protein inclusions. *Cell Rep.* **31**, 107680. doi:10.1016/j.celrep.2020.107680

Escusa-Toret, S., Vonk, W. I. M. and Frydman, J. (2013). Spatial sequestration of misfolded proteins by a dynamic chaperone pathway enhances cellular fitness during stress. *Nat. Cell Biol.* **15**, 1231-1243. doi:10.1038/ncb2838

Frottin, F., Schueder, F., Tiwary, S., Gupta, R., Körner, R., Schlichthaerle, T., Cox, J., Jungmann, R., Hartl, F. U., Hipp, M. S. et al. (2019). The nucleolus functions as a phase-separated protein quality control compartment. *Science* **365**, 342-347. doi:10.1126/science.aaw9157

Gallagher, P. S., Clowes Candadai, S. V. and Gardner, R. G. (2014). The requirement for Cdc48/p97 in nuclear protein quality control degradation depends on the substrate and correlates with substrate insolubility. *J. Cell Sci.* **127**, 1980-1991. doi:10.1242/jcs.141838

Gallina, I., Colding, C., Henriksen, P., Beli, P., Nakamura, K., Offman, J., Mathiasen, D. P., Silva, S., Hoffmann, E., Groth, A. et al. (2015). Cmr1/WDR76 defines a nuclear genotoxic stress body linking genome integrity and protein quality control. *Nat. Commun.* **6**, 6533. doi:10.1038/ncomms7533

Galy, V., Gadal, O., Fromont-Racine, M., Romano, A., Jacquier, A. and Nehrbass, U. (2004). Nuclear retention of unspliced mRNAs in yeast is mediated by perinuclear Mlp1. *Cell* **116**, 63-73. doi:10.1016/S0092-8674(03)01026-2

Hartl, F. U., Bracher, A. and Hayer-Hartl, M. (2011). Molecular chaperones in protein folding and proteostasis. *Nature* **475**, 324-332. doi:10.1038/nature10317

Ho, C.-T., Grousl, T., Shatz, O., Jawed, A., Ruger-Herreros, C., Semmelink, M., Zahn, R., Richter, K., Bukau, B., Mogk, A. et al. (2019). Cellular sequestrases maintain basal Hsp70 capacity ensuring balanced proteostasis. *Nat. Commun.* **10**, 4851. doi:10.1038/s41467-019-12868-1

Kaganovich, D., Kopito, R. and Frydman, J. (2008). Misfolded proteins partition between two distinct quality control compartments. *Nature* **454**, 1088-1095. doi:10.1038/nature07195

Khmelinskii, A., Keller, P. J., Bartosik, A., Meurer, M., Barry, J. D., Mardin, B. R., Kaufmann, A., Trautmann, S., Wachsmuth, M., Pereira, G. et al. (2012). Tandem fluorescent protein timers for in vivo analysis of protein dynamics. *Nat. Biotechnol.* **30**, 708-714. doi:10.1038/nbt.2281

Kumar, R., Nawroth, P. P. and Tyedmers, J. (2016). Prion aggregates are recruited to the insoluble protein deposit (IPOD) via Myosin 2-based vesicular transport. *PLoS Genet.* **12**, e1006324. doi:10.1371/journal.pgen.1006324

Leung, G. P., Brown, J. A. R., Glover, J. N. M. and Kobor, M. S. (2016). Rtt107 BRCT domains act as a targeting module in the DNA damage response. *DNA Repair* **37**, 22-32. doi:10.1016/j.dnarep.2015.10.007

Li, Z., Vizeacoumar, F. J., Bahr, S., Li, J., Warringer, J., Vizeacoumar, F. S., Min, R., Vandersluis, B., Bellay, J., Devit, M. et al. (2011). Systematic exploration of essential yeast gene function with temperature-sensitive mutants. *Nat. Biotechnol.* **29**, 361-367. doi:10.1038/nbt.1832

Luisier, R., Tyzack, G. E., Hall, C. E., Mitchell, J. S., Devine, H., Taha, D. M., Malik, B., Meyer, I., Greensmith, L., Newcombe, J. et al. (2018). Intron retention and nuclear loss of SFPQ are molecular hallmarks of ALS. *Nat. Commun.* **9**, 2010. doi:10.1038/s41467-018-04373-8

Maric, M., Mukherjee, P., Tatham, M. H., Hay, R. and Labib, K. (2017). Ufd1-Npl4 Recruit Cdc48 for disassembly of ubiquitylated CMG helicase at the end of chromosome replication. *Cell Rep.* **18**, 3033-3042. doi:10.1016/j.celrep.2017.03.020

Mathew, V., Tam, A. S., Milbury, K. L., Hofmann, A. K., Hughes, C. S., Morin, G. B., Loewen, C. J. R. and Stirling, P. C. (2017). Selective aggregation of the splicing factor Hsh155 suppresses splicing upon genotoxic stress. *J. Cell Biol.* **216**, 4027-4040. doi:10.1083/jcb.201612018

Miller, S. B. M., Ho, C.-T., Winkler, J., Khokhrina, M., Neuner, A., Mohamed, M. Y. H., Guilbride, D. L., Richter, K., Lisby, M., Schiebel, E. et al. (2015). Compartment-specific aggregases direct distinct nuclear and cytoplasmic aggregate deposition. *EMBO J.* **34**, 778-797. doi:10.15252/embj.201489524

Pantazopoulou, M., Boban, M., Foisner, R. and Ljungdahl, P. O. (2016). Cdc48 and Ubx1 participate in a pathway associated with the inner nuclear membrane that governs Asi1 degradation. *J. Cell Sci.* **129**, 3770-3780. doi:10.1242/jcs.189332

Psakhye, I. and Jentsch, S. (2012). Protein group modification and synergy in the SUMO pathway as exemplified in DNA repair. *Cell* **151**, 807-820. doi:10.1016/j.cell.2012.10.021

Ruan, L., Zhou, C., Jin, E., Kucharavy, A., Zhang, Y., Wen, Z., Florens, L. and Li, R. (2017). Cytosolic proteostasis through importing of misfolded proteins into mitochondria. *Nature* **543**, 443-446. doi:10.1038/nature21695

Saarikangas, J. and Barral, Y. (2016). Protein aggregation as a mechanism of adaptive cellular responses. *Curr. Genet.* **62**, 711-724. doi:10.1007/s00294-016-0596-0

Saugar, I., Jiménez-Martín, A. and Tercero, J. A. (2017). Subnuclear relocalization of structure-specific endonucleases in response to DNA damage. *Cell Rep.* **20**, 1553-1562. doi:10.1016/j.celrep.2017.07.059

Sherman, F. (2002). Getting started with yeast. *Methods Enzymol.* **350**, 3-41. doi:10.1016/s0076-6879(02)50954-x

Simões, T., Schuster, R., den Brave, F. and Escobar-Henriques, M. (2018). Cdc48 regulates a deubiquitylase cascade critical for mitochondrial fusion. *eLife* **7**, e30015. doi:10.7554/eLife.30015

Sontag, E. M., Vonk, W. I. M. and Frydman, J. (2014). Sorting out the trash: the spatial nature of eukaryotic protein quality control. *Curr. Opin. Cell Biol.* **26**, 139-146. doi:10.1016/j.ceb.2013.12.006

Stirling, P. C., Bloom, M. S., Solanki-Patil, T., Smith, S., Sipahimalani, P., Li, Z., Kofoed, M., Ben-Aroya, S., Myung, K., Hieter, P. et al. (2011). The complete spectrum of yeast chromosome instability genes identifies candidate CIN cancer genes and functional roles for ASTRA complex components. *PLoS Genet.* **7**, e1002057. doi:10.1371/journal.pgen.1002057

Tam, A. S., Sihota, T. S., Milbury, K. L., Zhang, A., Mathew, V. and Stirling, P. C. (2019). Selective defects in gene expression control genome instability in yeast splicing mutants. *Mol. Biol. Cell* **30**, 191-200. doi:10.1091/mbc.E18-07-0439

Thattikota, Y., Tollis, S., Palou, R., Vinet, J., Tyers, M. and D'Amours, D. (2018). Cdc48/VCP promotes chromosome morphogenesis by releasing condensin from self-entrapment in chromatin. *Mol. Cell* **69**, 664-676.e5. doi:10.1016/j.molcel.2018.01.030

Tkach, J. M., Yimit, A., Lee, A. Y., Riffle, M., Costanzo, M., Jaschob, D., Hendry, J. A., Ou, J., Moffat, J., Boone, C. et al. (2012). Dissecting DNA damage response pathways by analysing protein localization and abundance changes during DNA replication stress. *Nat. Cell Biol.* **14**, 966-976. doi:10.1038/ncb2549

Ulrich, H. D. and Davies, A. A. (2009). In vivo detection and characterization of sumoylation targets in Saccharomyces cerevisiae. *Methods Mol. Biol.* **497**, 81-103. doi:10.1007/978-1-59745-566-4_6
Verma, R., Oania, R., Fang, R., Smith, G. T. and Deshaies, R. J. (2011). Cdc48/p97 mediates UV-dependent turnover of RNA Pol II. *Mol. Cell* **41**, 82-92. doi:10.1016/j.molcel.2010.12.017
Wallace, E. W. J., Kear-Scott, J. L., Pilipenko, E. V., Schwartz, M. H., Laskowski, P. R., Rojek, A. E., Katanski, C. D., Riback, J. A., Dion, M. F., Franks, A. M. et al. (2015). Reversible, specific, active aggregates of endogenous proteins assemble upon heat stress. *Cell* **162**, 1286-1298. doi:10.1016/j.cell.2015.08.041
Yoshida, K. and Ogawa, S. (2014). Splicing factor mutations and cancer. *Wiley Interdiscip. Rev. RNA* **5**, 445-459. doi:10.1002/wrna.1222
Zhou, C., Slaughter, B. D., Unruh, J. R., Guo, F., Yu, Z., Mickey, K., Narkar, A., Ross, R. T., McClain, M., Li, R. et al. (2014). Organelle-based aggregation and retention of damaged proteins in asymmetrically dividing cells. *Cell* **159**, 530-542. doi:10.1016/j.cell.2014.09.026

Supplementary Information

Figure S1. Additional control experiments and characterization of the *cdc48-ts* alleles. (A) Representative images of Cdc48-GFP foci relative to HTA2-mCherry staining of yeast nuclei. White arrows indicate INQ, yellow arrows indicate CytoQ. (B) Co-staining of Cdc48-GFP with the INQ marker Hos2-mCherry in the indicated chaperone mutant strains. Representative images are shown above, and quantification of foci are shown below. **p<0.01, ***p<0.001. Error bars are mean± SEM, n= 3 with >50 cells each. Two-way ANOVA with Dunnett's test. (C) Spot dilution assay showing growth sensitivity of different *cdc48-ts* mutant alleles tested at the indicated temperatures. Equal ODs of the indicated strains were serially diluted and spotted on YPD at 25°C, 30°C, 34°C and 37°C. (D) Spontaneous Hos2-GFP foci formation in the *cdc48-4* mutant strain. (E) Schematic of Cdc48 protein domains (N- N-terminal, D1, D2 and Ct- C terminal) with indicated *cdc48-2, -3* and *-4* coding mutations (red lines) mapped along the sequence. (F) Hsh155-GFP foci induction in WT or *san1*Δ strains treated with MMS. Error bars are mean± SEM, n= 3 with >50 cells each. Fisher test, non-significant (ns). (G) Representative images for quantification of tandem fluorescent timer (tFT) analysis of Hsh155-mCherry-GFP dual fusion protein as shown in **Figure 4B.** Dotted inlets represent the nuclear region scored for the tFT ratios. (H) tFT ratio scoring of nuclear versus peripheral foci fluorescence in the indicated strains with or without MMS. Quantification of fluorescent timer indicates aggregation of older proteins in both INQ and CytoQ of cdc48-4 compared to WT in both conditions. Mean± SEM, three replicates, n ≥ 30 per replicate, Mann-Whitney test, asterisks show p-value threshold **** p<0.0001; non-significant (ns).

Mathew_ SupFig1

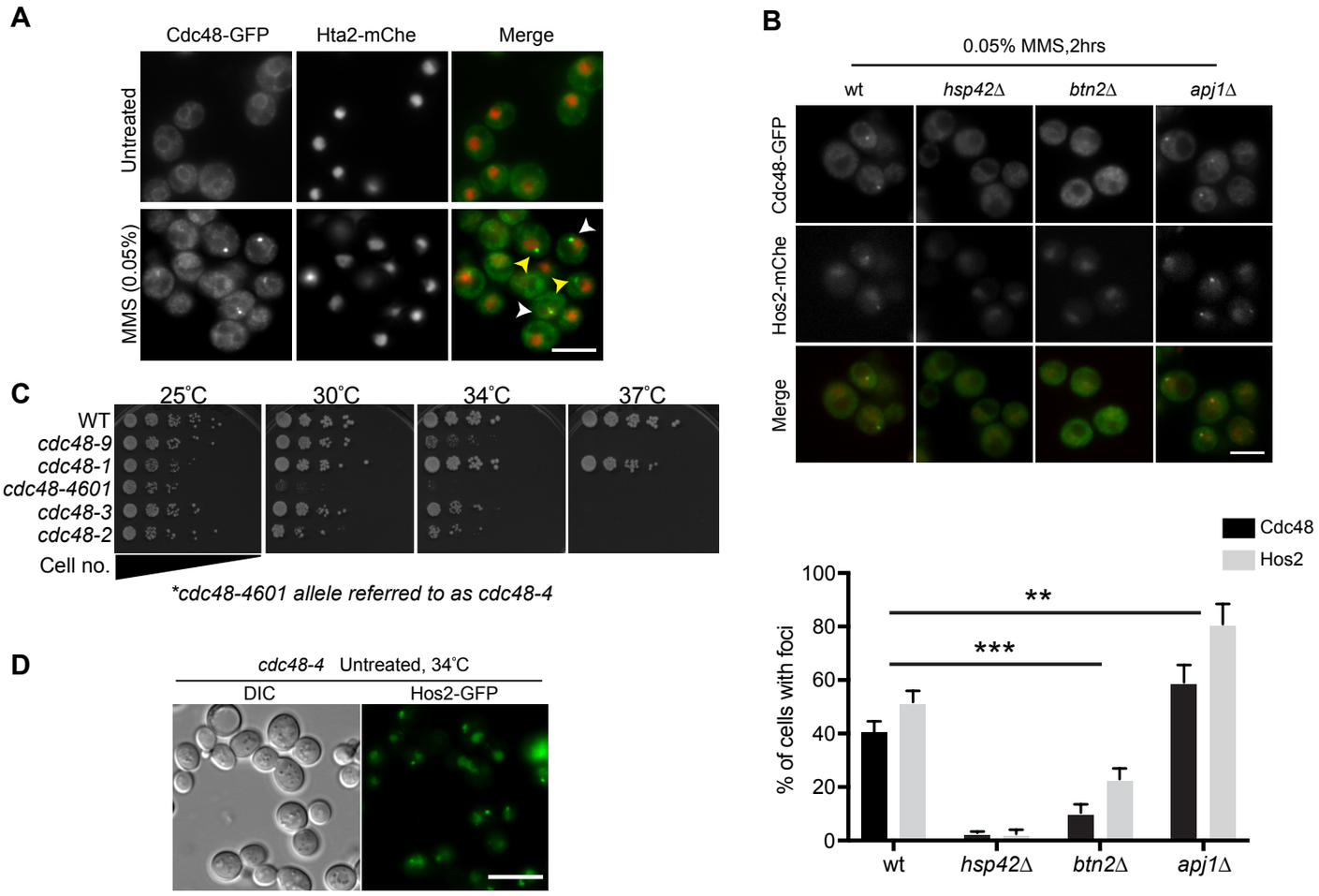

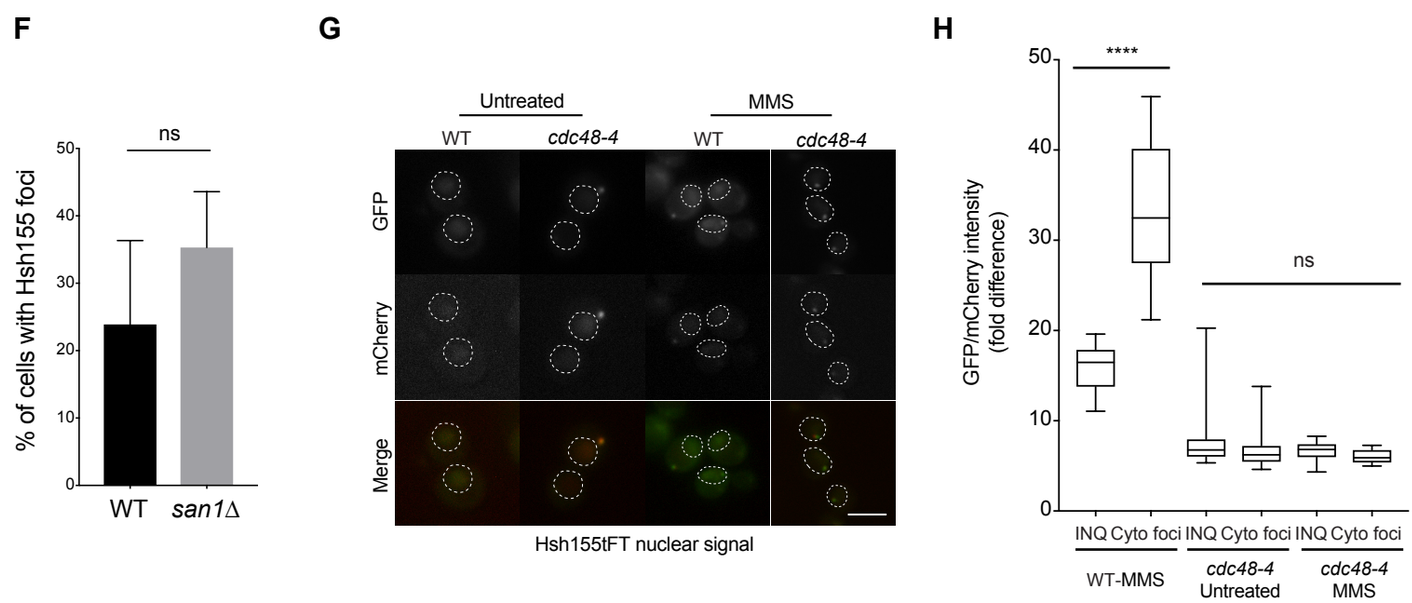

Table S1. Yeast strains, primers, and plasmids used in this study

Yeast strains* used in this study

*All strains are derivatives of s288c

Strain description	Strain number	Relevant genotype	Source
BY4741	PSY153	MATa *ura3Δ0 leu2Δ0 his3Δ1 met15Δ0*	J. Boeke, New York University, New York, NY
Cdc48-GFP	PSY1449	MATa *ura3Δ0 leu2Δ0 met15Δ0 or MET15 CDC48-GFP::HIS3*	B. Andrews, University of Toronto, Toronto, Ontario, Canada
Hsh155-GFP	PSY1502	MATa *ura3Δ0 leu2Δ0 met15Δ0 or MET15 HSH155-GFP::HIS3*	B. Andrews
Cdc48-GFP, Hos2-mCherry	PSYL1087	MATa *ura3Δ0 leu2Δ0 met15Δ0 or MET15 CDC48-GFP::HIS3 HOS2-mCherry::CaURA3*	This study
hsp42Δ, Cdc48-GFP	PSYL727	MATa leu2Δ0 met15Δ0 or MET15 ura3Δ0 hsp42Δ::KanMX CDC48-GFP::HIS3	This study
btn2Δ,Cdc48-GFP	PSYL725	MATa leu2Δ0 met15Δ0 or MET15 ura3Δ0 btn2Δ::KanMX CDC48-GFP::HIS3	This study
apj1Δ,Cdc48-GFP	PSYL718	MATa leu2Δ0 met15Δ0 or MET15 ura3Δ0 apj1Δ::KanMX CDC48-GFP::HIS3	This study
cdc48-4601-ts, Hsh155-GFP	PSYL721	MATa leu2Δ0 met15Δ0 or MET15 ura3Δ0 *cdc48-4601ts::KanMX HSH155-GFP::HIS3*	This study
cdc48-2-ts, Hsh155-GFP	PSYL991	MATa leu2Δ0 met15Δ0 or MET15 ura3Δ0 *cdc48-2ts::KanMX HSH155-GFP::HIS3*	This study
cdc48-3-ts, Hsh155-GFP	PSYL996	MATa leu2Δ0 met15Δ0 or MET15 ura3Δ0 *cdc48-3ts::KanMX HSH155-GFP::HIS3*	This study
Hsh155-mCherry-sfGFP	PSYL733	MATa *ura3Δ0 leu2Δ0 his3Δ1 met15Δ0 HSH155-mCherry-sfGFP::KanMX*	This study, Gallina et al., 2015
cdc48-4601-ts, Hsh155-mCherry-sfGFP	PSYL1216	MATa *ura3Δ0 leu2Δ0 his3Δ1 met15Δ0 HSH155-mCherry-sfGFP::HygMX cdc48-4601ts::KanMX*	This study
Hsh155-GFP, Cdc48-TAP	PSYL1125	MATα *leu2Δ0 met15Δ0 or MET15 ura3Δ0 CDC48-TAP::HIS3 HSH155-GFP::HIS3*	This study

Cdc48-GFP, Hsh155-TAP	PSYL1088	MATα *leu2Δ0 met15Δ0 or MET15 ura3Δ0 HSH155-TAP::HIS3 CDC48-GFP::HIS3*	This study
cdc48-4601-ts, Hsh155-GFP, Cus1-TAP	PSYL1002	MATa *leu2Δ0 met15Δ0 or MET15 ura3Δ0 CUS1-TAP::HIS3 HSH155-GFP::HIS3 cdc48-4601ts::KanMX*	This study
Hsh155-GFP, Cus1-TAP	PSYL881	MATα *leu2Δ0 met15Δ0 or MET15 ura3Δ0 CUS1-TAP::HIS3 HSH155-GFP::HIS3*	This study
cdc48-4601-ts, Hos2-GFP	PSYL723	*MATa leu2Δ0 met15D0 or MET15 ura3Δ0 cdc48-4601ts::KanMX HOS2-GFP::HIS3*	This study
san1Δ, Hsh155-GFP	PSYL1097	MATα *leu2Δ0 met15Δ0 or MET15 ura3Δ0 san1Δ::KanMX HSH155-GFP::HIS3*	This study
ubc9-1-ts, Hsh155-GFP	PSYL873	MATα *leu2Δ0 met15Δ0 or MET15 ura3Δ0 ubc9-1::KanMX HSH155-GFP::HIS3*	This study
siz1Δ, Hsh155-GFP	PSYL1218	MATa *leu2Δ0 met15Δ0 or MET15 ura3Δ0 siz1Δ::KanMX HSH155-GFP::HIS3*	This study
cdc48-4601-ts, siz1Δ, Hsh155-GFP	PSYL1301	MATa *leu2Δ0 met15Δ0 or MET15 ura3Δ0 cdc48-4601ts::KanMX siz1Δ::KanMX HSH155-GFP::HIS3*	This study
cdc48-4601-ts, pCDC48, Hsh155-GFP	PSYL1380	MATα *leu2-112-URA3-leu2-k; cdc48-4601ts::KanMX; pYC: TRP1 CDC48 HSH155-GFP::HIS3*	This study, Bergink et al., 2013
cdc48-4601-ts, pcdc48^{SIMmut} , Hsh155-GFP	PSYL1382	MATα *leu2-112-URA3-leu2-k; cdc48-4601ts::KanMX; pYC: TRP1 cdc48^{SIMmut} HSH155-GFP::HIS3*	This study, Bergink et al., 2013
btn2Δ, Cdc48-GFP, Hos2-mCherry	PSYL1594	MATa *ura3Δ0 leu2Δ0 met15Δ0 or MET15 btn2Δ::KanMX CDC48-GFP::HIS3 HOS2-mCherry::CaURA3*	This study
hsp42Δ, Cdc48-GFP, Hos2-mCherry	PSYL1595	MATa *ura3Δ0 leu2Δ0 met15Δ0 or MET15 hsp42Δ::KanMX CDC48-GFP::HIS3 HOS2-mCherry::CaURA3*	This study
apj1Δ,Cdc48-GFP, Hos2-mCherry	PSYL1596	MATa *ura3Δ0 leu2Δ0 met15Δ0 or MET15 apj1Δ::KanMX CDC48-GFP::HIS3 HOS2-mCherry::CaURA3*	This study
Cdc48-GFP, Hta2-mCherry	PSYL1537	MATa *ura3Δ0 leu2Δ0 met15Δ0 or MET15 CDC48-GFP::HIS3 HTA2-mCherry::HygMX*	This study

Primers used in this study

Primer name		Primer sequence (5'-3')	Primer description
Hsh155-tFT-F		CCCCGTTACACCAGACAACAATGAAGAATATATAGAAGAACTGGATTTAGTTCTGCGTACGCTGCAGGTCGAC	PCR-based homologous recombination to insert mCherry-sfGFP to Hsh155
Hsh155-tFT-R		GTCAAGTAAAATATTCTTACAAGTTGTGGTTATTTATATGCTCTATATATATTCAATCGATGAATTCGAGCTCG	PCR-based homologous recombination to insert mCherry-sfGFP to Hsh155
Cdc48-1-600-F		CTGGGAAGGTGAGCCAATCAACAGG	Forward sequencing primers for 1-600bp of Cdc48
Cdc48-600-1200-F		CTGATGATGTTGATTTGGAAGCATTGG	Forward sequencing primers for 600-1200bp of Cdc48
Cdc48-1200-1800-F		CGGATAGAGTCGTCAACCAACTATTAAC	Forward sequencing primers for 1200-1800bp of Cdc48

Plasmids used in this study

Plasmid description		Relevant Features	Source
pMaM17		*AMP^R mCherry-sfGFP-KanMX*	Khmelinskii et al., 2012
pJCR51- intron version of LacZ gene (for splicing efficiency)		*AMP^R CEN pJCR51::LEU2*	Galy et al., 2004
pLGSD5- intronless version of LacZ gene (used for normalization)		*AMP^R CEN pLGSD5::LEU2*	Galy et al., 2004
pRG3094		*AMP^R CEN pRG3094-cdc48-myc::URA3*	Gallagher et al., 2014
pRG4061		*AMP^R CEN pRG3094-cdc48^{E315Q}-myc::URA3*	Gallagher et al., 2014
YEplac181		*AMP^R CUP1 YEplac181-HIS-Smt3::LEU2*	Ulrich et al., 2009 (obtained from Addgene)